catalysts

MDPI

Article

Bimetallic Metal-Organic Framework Derived Nanocatalyst for CO_2 Fixation through Benzimidazole Formation and Methanation of CO_2

Aasif Helal [1,*], Mohammed Ahmed Sanhoob [1], Bosirul Hoque [1], Muhammad Usman [1] and Md. Hasan Zahir [2]

[1] Interdisciplinary Research Center for Hydrogen and Energy Storage, King Fahd University of Petroleum & Minerals, Dhahran 31261, Saudi Arabia
[2] Interdisciplinary Research Center for Renewable Energy and Power Systems, King Fahd University of Petroleum & Minerals, Dhahran 31261, Saudi Arabia
* Correspondence: aasifh@kfupm.edu.sa; Tel.: +966-013-860-7532

Abstract: In this paper, a bimetallic Metal-Organic Framework (MOF) CoNiBTC was employed as a precursor for the fabrication of bimetallic nanoalloys CoNi@C evenly disseminated in carbon shells. These functional nanomaterials are characterized by powdered X-ray diffraction (PXRD), Fourier Transform Infra-Red spectroscopy (FTIR), surface area porosity analyzer, X-ray photoelectron spectroscopy (XPS), Field emission scanning electron microscopy (FESEM), Transmission electron microscopy (TEM), Hydrogen Temperature-Programmed Reduction (H_2 TPR), CO_2 Temperature-Programmed Desorption (CO_2-TPD), and Inductively Coupled Plasma Mass Spectrometry (ICP-MS). This nanocatalyst was utilized in the synthesis of benzimidazole from *o*-phenylenediamine in the presence of CO_2 and H_2 in a good yield of 81%. The catalyst was also efficient in the manufacture of several substituted benzimidazoles with high yield. Due to the existence of a bimetallic nanoalloy of Co and Ni, this catalyst was also employed in the methanation of CO_2 with high selectivity (99.7%).

Keywords: Metal-Organic Framework; bimetallic; nanoalloy; benzimidazole; methanation

check for updates

Citation: Helal, A.; Sanhoob, M.A.; Hoque, B.; Usman, M.; Zahir, M.H. Bimetallic Metal-Organic Framework Derived Nanocatalyst for CO_2 Fixation through Benzimidazole Formation and Methanation of CO_2. *Catalysts* **2023**, *13*, 357. https://doi.org/10.3390/catal13020357

Academic Editor: Zhixin Yu

Received: 31 December 2022
Revised: 27 January 2023
Accepted: 30 January 2023
Published: 6 February 2023

Copyright: © 2023 by the authors. Licensee MDPI, Basel, Switzerland. This article is an open access article distributed under the terms and conditions of the Creative Commons Attribution (CC BY) license (https://creativecommons.org/licenses/by/4.0/).

1. Introduction

Rapid industrialization during the last few years and the high energy demand of our society have disrupted the equity in the planet's climate and ecosystem. In global energy consumption, conventional sources provide 78% while the remaining 22% is achieved from renewable energy [1–3]. The use of conventional energy sources leaves a colossal carbon footprint in our environment. Carbon dioxide (CO_2) is one of the dominant greenhouse gases, and its escalating amount has an adverse impact on the climate and living organisms, such as severe weather changes, food shortage, and migration of animals [4]. Several measures have been undertaken to mitigate CO_2 emissions and develop new energy alternatives [5–8]. The chemical conversion of CO_2 into value-added products such as formic acid, methanol, carbonates, methane, and amides through the C-H, C-O, C-C, and C-N bonds has engrossed much attention, since CO_2 is a nontoxic, bountiful, economical, and renewable C1 resource and its utilization is relevant for sustainable development [9–16]. But due to high thermodynamic stability and chemically inert nature, catalysts are required for the activation of the CO_2 for the chemical transformations. Benzimidazole is a versatile N-containing heterocyclic skeleton that is extensively used in the synthesis of pesticides, pharmaceuticals, and materials [17–19]. The general strategy involved in the formation of benzimidazole is the merger of a C1 source with a diamine to form two C-N bonds through reductive cyclization. Several compounds such as N, N-dimethylformamide, dimethoxyethane, formic acid, and methanol have been used as a C1 resource. However, they are found to be expensive and toxic in nature as compared to CO_2 as a sustainable, economical, and nontoxic C1 source. The conversion of CO_2 to methane is also a considerable chemical process that can mitigate CO_2 emission. Different types of metal catalysts based on Ru, Rh, Pd, Co, and Ni have been applied as competent materials for heterogeneous

CO_2 methanation [20–22]. But most of these catalysts are expensive and some suffer from stability issues at elevated temperatures and pressure.

Transitional metals (Ni, Co, and Fe) have been extensively used to design these catalysts instead of noble metals (Pt, Pd, Rh) due to their expensive nature, low abundance, and limited industrial application [23,24]. However, these monometallic transitional metal catalysts also suffer from deactivation, metal particle sintering, and regeneration of the catalysts [25]. Thus, bimetallic or alloy catalysts showed substantially different properties than their monometallic analogs due to the synergistic effects of the two metals [26].

Metal-Organic Frameworks (MOFs) and their derivatives have become essential materials for heterogeneous catalysis over the past three decades [27]. However, under harsh reaction conditions with elevated temperatures the stability, efficiency, and recyclability of the catalyst are not achievable. Through direct carbonization of MOF under an inert atmosphere at a pertinent temperature, however, carbon-supported metal/metal oxide catalysts can be derived that have a higher tolerance against strident reaction conditions [28]. Furthermore, mixed metal MOFs after the annealing process can result in MOF-derived porous bimetallic@C composites that render highly dispersed specific metal nanoparticles enclosed in carbon shells. This exclusive configuration of metal@carbon hybrid provides bimetallic nanoparticles for catalysis and prevents the aggregation of metal nanoparticles at high temperatures [29]. Thus, in this paper, we prepared a bimetallic nanoalloy (CoNi@C) of Co and Ni derived from a bimetallic MOF (CoNiBTC). We investigated how this bimetallic catalyst (CoNi@C) can assist in CO_2 fixation through benzimidazole formation and methanation of CO_2.

2. Results and Discussion

The synthesis of bimetallic CoNiBTC precursor was carried out following a slightly modified method, as mentioned in the literature for the synthesis of CoBTC MOF [30]. An equimolar ratio of cobalt nitrate and nickel nitrate were dissolved with trimesic acid in dimethylformamide as the solvent and acetic acid as a modulator and heated at 448 K for 72 h. Similarly, by varying the ratio of cobalt nitrate and nickel nitrate, CoNiBTC-1 and CoNiBTC-2 were prepared. Furthermore, CoBTC and NiBTC were synthesized using the procedure described in the literature. The MOFs obtained were washed several times by solvent exchange and utilized as precursors for the design and synthesis of MOF-derived porous CoNi@C, CoNi@C-1, CoNi@C -2, Co@C, and Ni@C composites with well-dispersed Co and Ni nanoparticles, in different ratios, precisely enclosed in carbon shells. The powder XRD of the CoBTC, NiBTC, and CoNiBTC exhibited that all the MOFs are crystalline and the topologies are the same as the simulated CoBTC reported in the literature with characteristic peaks at $2\theta = 7.55°$, $11.02°$, and $12.81°$ [31]. The CoNiBTC-1 and CoNiBTC-2 exhibit similar distinctive peaks as well (Figure S1a). This signifies that the presence of nickel in the CoNiBTC does not disturb the topology or the phase purity of the CoBTC MOF (Figure 1a). After pyrolysis, Co@C, Ni@C, CoNi@C, CoNi@C-1, and CoNi@C-2 also displayed good crystallinity with the characteristic peaks for graphite ($2\theta = 30.6°$) and cubic phase of metallic Co, Ni, and Ni-Co ([111] [200] [220] facets) $2\theta = 44.4°$, $51.77°$ and $76.16°$ (Figure 1b and Figure S1b). The ICP-MS analysis of CoNiBTC revealed that the amounts of Co and Ni were 17% and 11%, respectively, while the amounts of metals in the CoNi@C were 35% and 23%. The bands at 710 cm^{-1} and 769 cm^{-1} in the FTIR spectrum of CoNiBTC (Figure S2) correspond to the linker's out-of-plane aromatic C-H bending modes. The peak at 1102 cm^{-1} is attributed to aromatic C-H in-plane bending, whereas the sharp peaks (1429, 1442 cm^{-1}) and (1561, 1608 cm^{-1}) are most likely due to the COO- group's symmetric and asymmetric C-O stretching modes [32]. The N_2 adsorption isotherm of the precursor CoNiBTC MOF displayed a sharp uptake at low pressure, indicating a type I isotherm with a completely microporous nature. The BET surface area was calculated to be 710 m^2g^{-1}. However, the N_2 adsorption isotherm of CoNi@C after pyrolysis showed a hysteresis loop within the P/Po range of 0.7–1, which is attributed to the material's micro-mesoporous nature. The surface area of CoNi@C was calculated to be 179 m^2/g. The

massive decrease in surface area is attributed to the annihilation of the MOF framework and a decrease in microporosity (Figure 2a). Figure 2b depicts the XPS spectrum of CoNi@C. The main characteristic peaks with binding energies for the metals were Co $2p_{3/2}$ at 778.8 eV (Co0) and Ni $2p_{3/2}$ at 852.8 eV (Ni0), which confirms the presence of the two metals in CoNi@C. The deconvoluted Co $2p_{3/2}$ data revealed three notable peaks at 778.8, 780.8, and 785.7 eV, which were indexed as Co°, the major peak, Co-O, and the satellite peak of the Co-O, respectively (Figure S3). Similarly, Ni $2p_{3/2}$ peaks fitted into three different peaks at around 852.5, 857.4, and 859.0 eV which are attributed to the Ni^0, the major peak, Ni^{2+}, and the satellite peak of Ni^{2+}, respectively (Figure S4). In addition, a graphitic carbon peak corresponding to sp^2 hybridization is detected at 284.3 eV. Temperature-programmed desorption of CO_2 (CO_2-TPD) was performed to determine the strength of surface basic sites for the bimetallic nanoalloy (CoNi@C) of Co and Ni. As depicted in Figure 3a, CoNi@C has a broad peak between 50–300 °C, indicating the existence of weak and moderate basic sites. A steep peak is also detected around 424 °C, which is related to the presence of strong basic sites. Thus, the catalyst has three weak, moderate, and strong basic sites that enhance CO_2 adsorption.

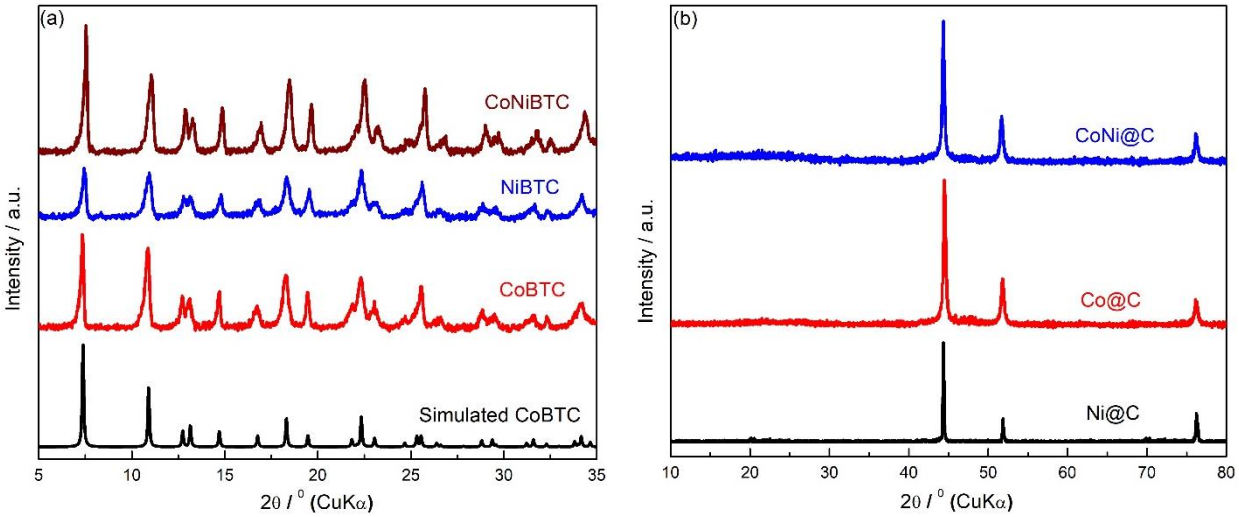

Figure 1. Pxrd of (**a**) CoNiBTC, CoBTC, and NiBTC; (**b**) CoNi@C, Ni@C, and Co@C.

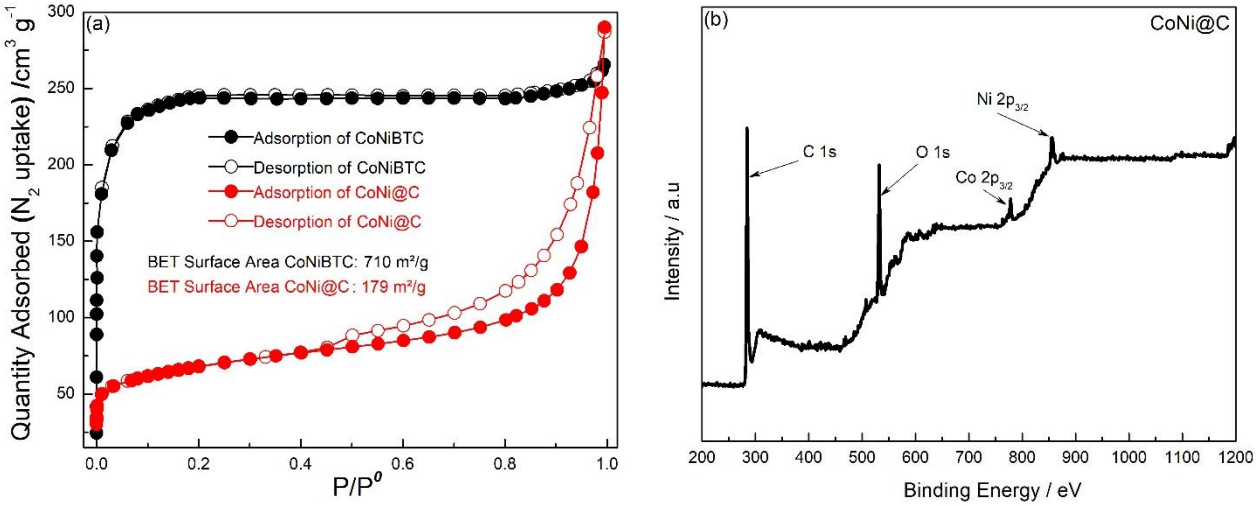

Figure 2. (**a**) The N_2 adsorption isotherm of CoNiBTC and CoNi@C; (**b**) XPS spectrum of CoNi@C.

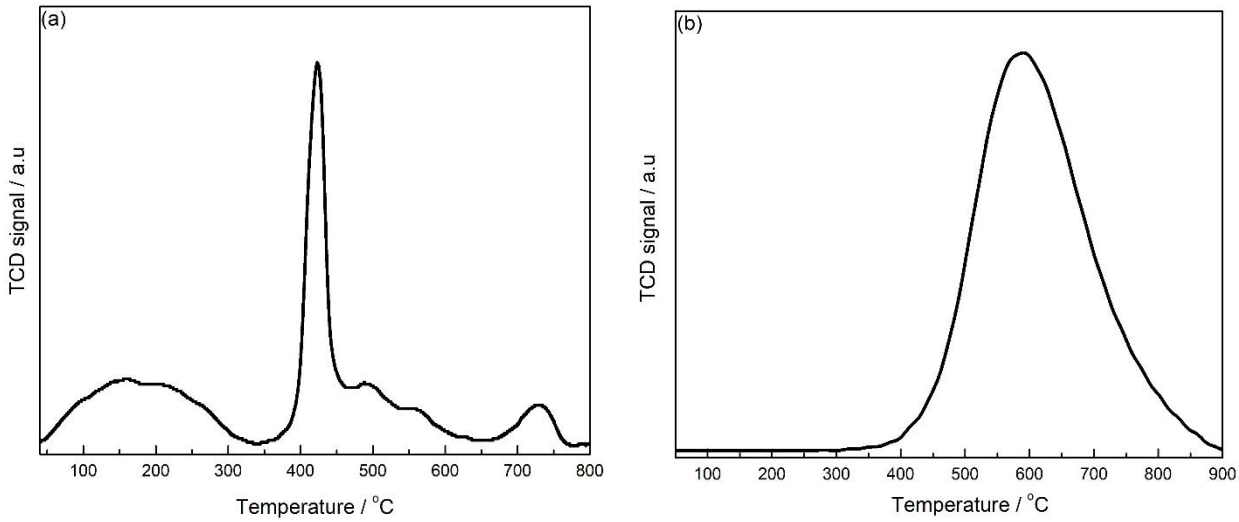

Figure 3. (**a**) CO_2-TPD; (**b**) H_2-TPR of CoNi@C.

Temperature-programmed reduction with hydrogen was used to determine the reducibility behavior of the Co and Ni bimetallic nanoalloy (CoNi@C). As reported previously, the presence of Ni in the Ni-Co alloy enhances the reducibility of the Cobalt [33]. As depicted in Figure 3b, a huge, broad peak centered at 590 °C was observed between 400–850 °C, indicating mixed CoO and NiO reduction to metals leading to more reducible species. FESEM data of the CoNiBTC showed hexagonal-shaped layered microcrystalline materials (Figure S5). EDX and elemental mapping analysis revealed that the Co/Ni ratio in the CoNiBTC MOF was 3:2 (Figure S6), which supports the ratio determined by the ICP-MS. TEM images of CoNi@C revealed a consistent distribution of Co-Ni nanoalloy with a size between 5 and 10 nm encased by a carbon layer. There was no discernible aggregate formation detected. Additionally, the particle lattice's average interplanar spacing was 0.21 nm, which is equivalent to the lattice spacing of nanoparticles made of the Co-Ni alloy (Figure 4) [34]. EDX analysis of the two bimetallic MOFs CoNiBTC-1 and CoNiBTC-2 indicated that the Co/Ni ratio was 1:1 in CoNiBTC-1 and 2:3 in CoNiBTC-2 (Figures S7–S10). Thus, from these MOFs, three bimetallic nanocatalysts with varying Co/Ni ratio, including CoNi@C (3:2), CoNi@C-1(1:1) and CoNi@C-2(2:3) were prepared.

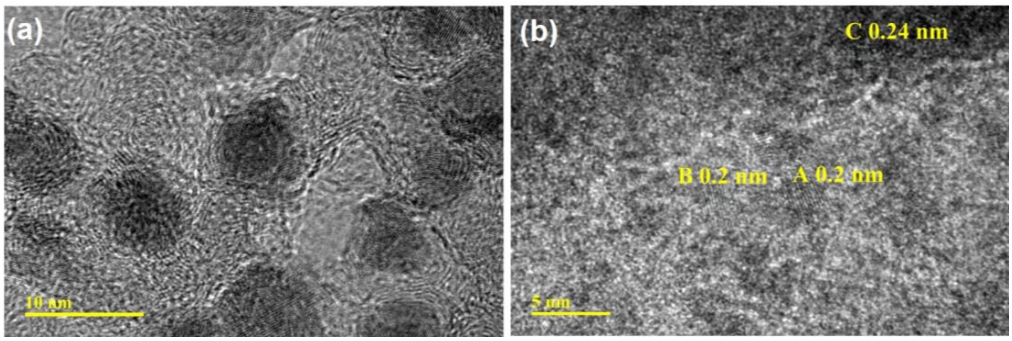

Figure 4. TEM of CoNi@C. (**a**) 10 nm and (**b**) 5 nm.

2.1. Catalysis

Synthesis of Benzimidazoles

The catalytic activities of CoNi@C were evaluated and the reaction conditions were optimized using *o*-phenylenediamine as the model substrate with CO_2 and H_2. A blank test was run in the absence of catalysts, and no benzimidazole was produced (Table 1, entry 1). Similarly, no benzimidazole was produced in the presence of cobalt or nickel salts as catalysts. In the presence of the pristine bimetallic MOF CoNiBTC, the conversion is very low even at elevated temperatures (Table 1, entries 4 and 5). In addition, the conversion

to benzimidazole was examined in the presence of Ni@C and Co@C, which produced poor yields under identical conditions. This suggests that the bimetallic nanoalloy's synergistic impact enhances the conversion (Table 1, entries 6 and 7). Consequently, maximal yield is achieved by employing the catalyst CoNi@C (Table 1, entries 8). Additionally, the ratio of Co/Ni was altered, but the yield was less than expected (Table 1, entry 9 and 10), indicating that the ratio of CoNi@C is the most successful in the conversion to benzimidazole. The synthesis of benzimidazole from *o*-phenylenediamine was examined in depth utilizing CoNi@C as catalysts. Figure 5a illustrates the relationship between reaction temperature and benzimidazole yield. At constant pressure and reaction time, the yield of benzimidazole increased with increasing temperature and remained constant at a specific temperature. Furthermore, we investigated the effect of reaction duration on benzimidazole yield (Figure 5b). The yield was shown to rise with a reaction time up to 18 h, after which the yield remained constant. Encouraged by the preliminary results of benzimidazole synthesis, we studied the general applicability and adaptability of this catalyst in the synthesis of other substituted benzimidazoles. We studied the cyclization of a variety of structurally different phenylenediamine with different electron-donating and electron-withdrawing functional groups by CO_2 in the presence of H_2 catalyzed by CoNi@C. Regardless of the substituents, the corresponding substituted benzimidazole derivatives were produced in a good yield (Table 2). This demonstrates conclusively that substituted groups have no effect on the cyclization of substrates by CO_2 in the presence of H_2 and CoNi@C as the catalyst. All the products were characterized by ^{1}H NMR and ^{13}C NMR (Section S2 and Figures S11–S14, SI). We also explored the regeneration of the catalyst in the benzimidazole synthesis and discovered that the catalyst could be regenerated for up to eight cycles (Figure 6) without any loss of crystallinity, as evidenced by the powdered XRD (Figure S14) and morphology as seen from the TEM (Figure S15).

Table 1. Synthesis of benzimidazole with different catalysts [a].

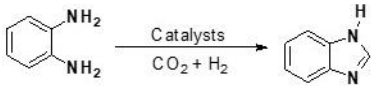

Entry	Catalysts	Temperature/°C	Yield/% [b]
1	—-	115	0
2	$Ni(NO_3)_26H_2O$	115	0
3	$Co(NO_3)_26H_2O$	115	0
4	CoNiBTC	115	9
5	CoNiBTC	130	11
6	Co@C	115	40
7	Ni@C	115	33
8	CoNi@C	115	81
9	CoNi@C-1	115	52
10	CoNi@C-2	115	38

[a] Reaction conditions: *o*-phenylenediamine, 1.0 mmol; pressure, 30 bar; time, 18 h. [b] Isolated yield calculated from the ^{1}HNMR.

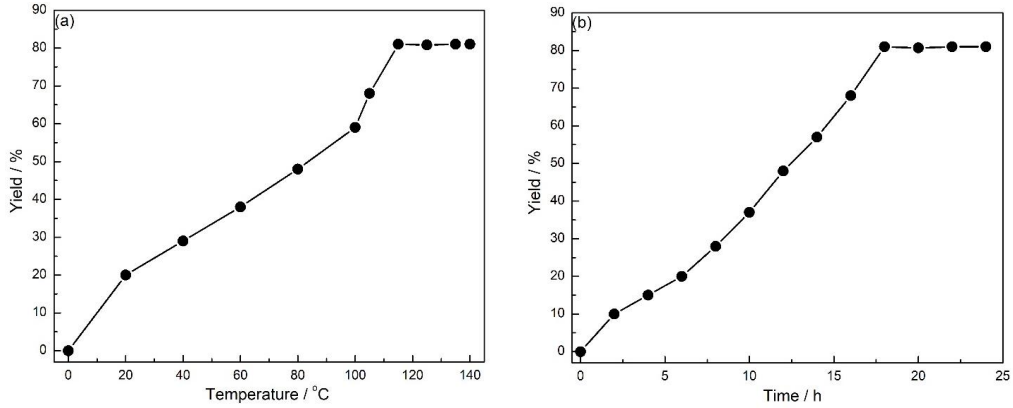

Figure 5. Influence of (**a**) temperature; and (**b**) reaction time on the yield of benzimidazole. Reaction conditions: *o*-phenylenediamine, 1.0 mmol; pressure, 30 bar; CoNi@C, 100 mg.

Table 2. CoNi@C-catalyzed synthesis of various benzimidazoles [a].

Entry	Substrate	Product	Yield
1	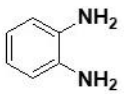	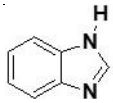	81
2	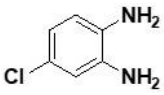	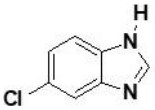	78
3	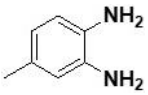	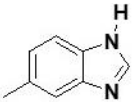	82
4	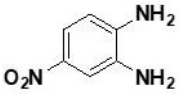	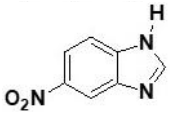	80

[a] Reaction conditions: substrates, 1.0 mmol; temperature, 115° C; pressure, 30 bar; time, 18 h.

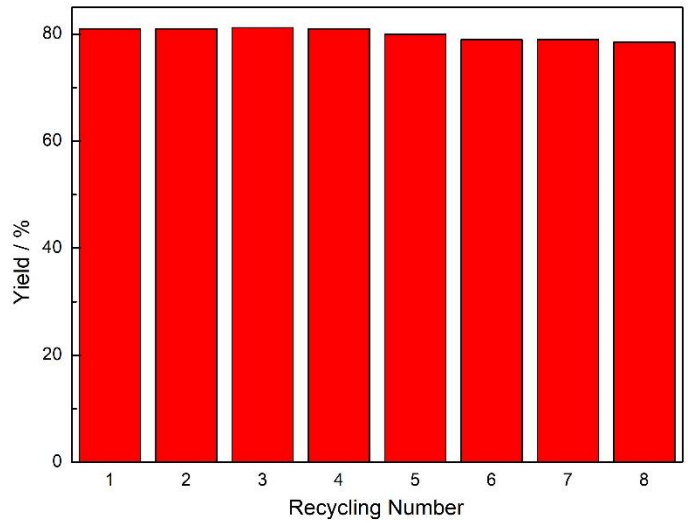

Figure 6. Recycle tests with CoNi@C for the reaction of benzimidazole synthesis.

From the mechanistic viewpoint, Figure 2 depicts the suggested reaction pathway for benzimidazole synthesis from *o*-phenylenediamine (1) cyclization by CO_2 in the presence of H_2. In principle, the reaction may proceed in two steps. In step one, the aromatic diamine

(1) acts as a base to facilitate the CO_2 hydrogenation to formic acid under the catalysis of CoNi@C. Subsequently, in step two, formamide (2) can be produced rapidly by dehydration of the diamine with formic acid, followed by intramolecular cyclization to the end product benzimidazole (3) (Figure 7). A literature review comparing similar types of catalysts used in the synthesis of benzimidazole revealed that our catalyst had a comparable yield under the corresponding reaction conditions (Table S4, SI).

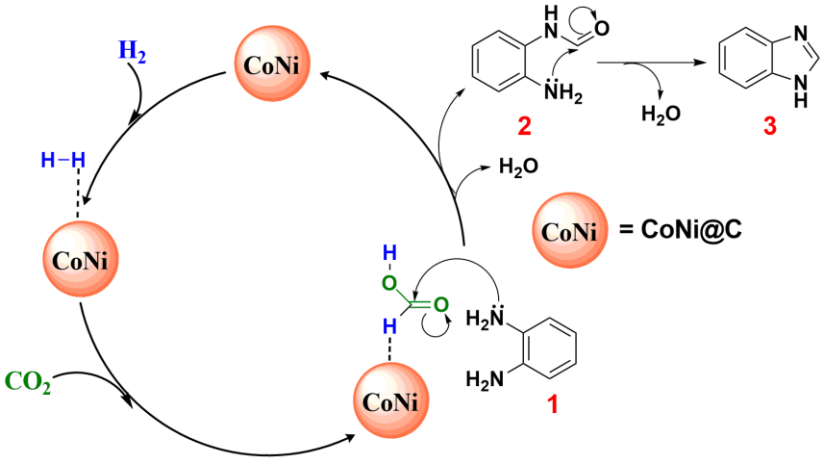

Figure 7. The plausible mechanism for benzimidazole formation catalyzed by CoNi@C.

2.2. Methanation of CO_2

The same catalyst was also explored for the methanation of CO_2. Numerous studies have demonstrated the importance of a nickel-based catalyst for the selectivity of methane. Supports such as aluminum oxide, titanium oxide, and cerium oxide are commonly employed in the methanation process [35]. In this work, a bimetallic nanoalloy (CoNi@C) of Co and Ni derived from a bimetallic MOF (CoNiBTC) was targeted to determine its stability and reactivity for CO_2 methanation (Scheme 1). As shown in Figure 8, it was observed that the conversion was around 23.8% at the first 1 h of reaction time. The conversion was enhanced to 39.0% after 360 min of reaction time, which indicates that the catalyst takes a long time to convert the large volume of reactant in the 27.8% after 600 min of reaction time. Selectivity, on the other hand, was very high toward methane. The selectivity of methane was above 99.7% during the reaction on the stream, which indicates that the bimetallic nanoalloy (CoNi@C) of Co and Ni is suitable for the methanation process. In order to comprehend the influence of pressure, we also conducted the same experiment at a lower pressure of 10 bar (Figure S17, SI), which resulted in a reduced 30% yield and 98% selectivity. We also investigated the influence of the Co/Ni ratio on the methanation reaction by using the CoNi@C-1 and CoNi@C-2. It was discovered that when the Co/Ni ratio is 1:1, conversion reduces to 23% while selectivity remains unchanged at 99% (Figure S18, SI). Alternatively, the same behavior was seen when the Co/Ni ratio was 2:3 (Figure S19, SI). A comparative study of the selectivity of several catalysts revealed that our catalyst was superior or comparable to others in terms of selectivity (Table S5, SI). In our laboratory, we are currently conducting more comprehensive research on the CO_2 hydrogenation of this catalyst on a variety of supports and with varying metal ratios and carbon content.

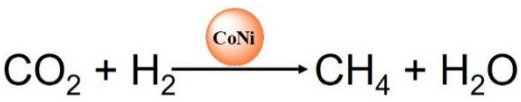

Scheme 1. The reaction of methanation with CO_2 and H_2.

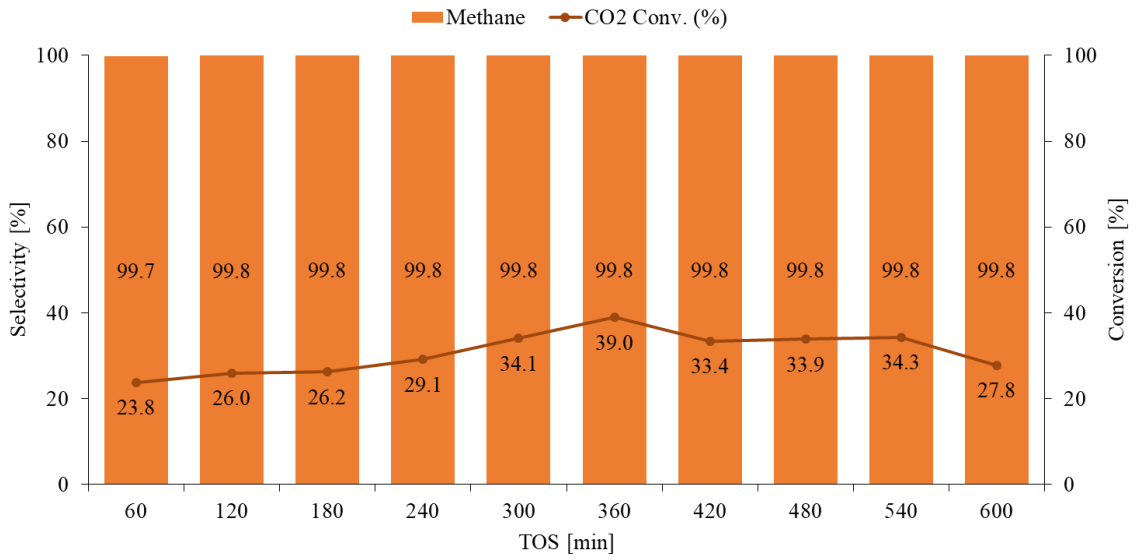

Figure 8. CoNi@C 0.2 g, flow of mixture = 15 mL, mixture (H_2: CO_2) = 3:1, T = 375 °C, 30 bar.

3. Experimental

3.1. Materials and General Methods

3.1.1. Chemicals used in This Work

Trimesic acid (98% purity) (TPA), Nickel nitrate hexahydrate (99.99% purity) ($Ni(NO_3)_2{\cdot}6H_2O$), Cobalt nitrate hexahydrate (99.99% purity) ($Co(NO_3)_2.6H_2O$) methanol (99.9% purity), *N*, *N*-dimethylformamide (DMF; 99.8% purity), Acetic acid (CH_3COOH) (99.0%) dichloromethane (99.8% extra-dry grade), *o*-Phenylenediamine (99.5%) with all the other derivatives of the aromatic diamines were purchased from Sigma Aldrich Corporation. NMR solvents: dimethyl sulfoxide-d_6 (DMSO-d_6; 99.9% purity) were purchased from Cambridge Isotope. All chemicals were used without further purification. Water used in this work was double-distilled and filtered through a Millipore membrane.

3.1.2. Instrumentation

^1H and ^{13}C NMR spectra were recorded on a Bruker AM-400 spectrometer using TMS as the internal standard. Powder X-ray diffraction (PXRD) patterns of the samples were recorded using a Rigaku MiniFlex diffractometer, which was equipped with Cu-K@ radiation. The data were acquired over the 2θ range of 5° and 40°. The FT-IR spectrum of the MOF was obtained using a Nicolet 6700 Thermo Scientific (Waltham, MA, USA) instrument in the range of 400–4000 cm^{-1}, using KBr. Thermogravimetric analysis (TGA) was conducted using a TA Q500 with the sample held in an alumina pan under airflow. The surface area was obtained from the nitrogen adsorption isotherm of the MOF using a Micromeritics (Norcross, GA, USA) ASAP 2020 instrument. A liquid nitrogen bath was used for the measurements at 77 K. The surface morphology of these materials was discerned using a field emission scanning electron microscope (FESEM, LYRA 3 Dual Beam, Tescan, Brno, Czech Republic), which operated at 30 kV. The FESEM samples were prepared from a suspension in ethanol. The surface chemical analyses were performed using an XPS equipped with an Al-Kα micro-focusing X-ray monochromator (ESCALAB 250Xi XPS Microprobe, Thermo Scientific, USA). Inductively Coupled Plasma Mass Spectrometry (ICP-MS) of the Cobalt- and Nickel-treated samples of CoNi@C were carried out in Thermo Scientific XSeries 2 ICP-MS. The catalysis for the benzimidazole formation was carried out in a Micro Batch Reactor System (PARR). Temperature-programmed reduction (TPR) and temperature-programmed desorption of CO_2 molecules (CO_2-TPD) were conducted using a BELCAT II (MicrotracBel, Osaka, Japan) analyzer. For H_2-TPR analysis, 50 mg of the catalyst was loaded and preheated under argon flow (50 mL/min) at 500 °C for 30 min. The sample was cooled down to 40 °C. After that, a mixture of hydrogen and argon

(10% H_2 in Ar, 50 mL/min) was passed over the catalyst, and the sample was heated to 900 °C at a ramping rate of 10 °C/min. The TCD signal was recorded simultaneously to determine the reducibility of the sample. For CO_2-TPD, the reduced sample was flushed with helium at 500 °C for 30 min and cooled down to room temperature. CO_2 gas was passed over the reduced sample at room temperature for 30 min (50 mL/min). After that, the sample was flushed with 50 mL/min of helium to remove the excess CO_2 for 30 min. Finally, the desorption of CO_2 was detected by the TCD detector during heating from room temperature to 800 °C at a ramping rate of 10 °C/min.

3.2. Synthesis of MOFs

3.2.1. Synthesis of CoBTC

The synthesis procedure was followed as specified in the literature [26].

3.2.2. Synthesis of NiBTC

The synthesis procedure was followed as specified in the literature [36].

3.2.3. Synthesis of CoNiBTC

CoNiBTC was synthesized by dissolving $Ni(NO_3)_{2.}$ $6H_2O$ (146 mg. 0.5 mmol), $Co(NO_3)_2$ (146 mg. 0.5 mmol), and Trimesic acid (210 mg. 1.0 mmol) in DMF (20 mL) with ultrasonic vibration for 15 min, then 5 mL of acetic acid was added. The as-obtained mixture was transferred to a 40 mL Parr steel autoclave and heated at 448 K for 72 h. Then the autoclave was cooled in the air to room temperature. The resulting microcrystalline powder was collected and washed with 3 × 10 mL of DMF for 3 days and 3 × 10 mL of CH_2Cl_2 for 3 days, yielding the required CoNiBTC in 55% yield (related to the metal salt). FT-IR (KBr, cm^{-1}): 3418, 1668, 1608, 1561, 1442, 1429, 1102, 769, 710, 674.

3.2.4. Synthesis of CoNiBTC-1

The synthesis method was identical to that of CoNiBTC. $Ni(NO_3)_{2.}$ $6H_2O$ (146 mg. 0.5 mmol), $Co(NO_3)_2$ (98 mg. 0.33 mmol), and Trimesic acid (210 mg. 1.0 mmol) in DMF (20 mL) with ultrasonic vibration for 15 min, then 5 mL of acetic acid was added. The as-obtained mixture was transferred to a 40 mL Parr steel autoclave and heated at 448 K for 72 h.

3.2.5. Synthesis of CoNiBTC-2

The synthesis method was identical to that of CoNiBTC. $Ni(NO_3)_{2.}$ $6H_2O$ (219 mg. 0.75 mmol), $Co(NO_3)_2$ (98 mg. 0.33 mmol), and Trimesic acid (210 mg. 1.0 mmol) in DMF (20 mL) with ultrasonic vibration for 15 min, then 5 mL of acetic acid was added. The as-obtained mixture was transferred to a 40 mL Parr steel autoclave and heated at 448 K for 72 h.

3.2.6. Synthesis of CoNi@C

The synthesized CoNiBTC (500 mg) was carbonized to produce CoNi@C. The pyrolysis process was performed in a quartz tubular reactor by loading the catalyst in the reactor tube. The sample was heated to 750 °C using nitrogen (25 mL/min) at a ramping rate of 5 °C/min, then held at that temperature for 8.0 h. The sample was then cooled to room temperature before being exposed to 5 mL/min of oxygen and 25 mL/min of nitrogen for two hours.

3.2.7. Synthesis of CoNi@C-1

Carbonized CoNi@C-1 was made from CoNiBTC-1 using the same method described above.

3.2.8. Synthesis of CoNi@C-2

The same procedure as described above was used to prepare carbonized CoNi@C-2 from CoNiBTC-2.

3.2.9. Synthesis of Co@C

The same procedure as described above was used to prepare carbonized Co@C from CoBTC.

3.2.10. Synthesis of Ni@C

Carbonized Co@C was made from CoBTC using the same method described above.

3.3. Catalysis of Benzimidazole Synthesis

The cyclization reaction of ortho-substituted aniline with CO_2/H_2 was performed in a 10 mL high-pressure Micro Batch Reactor System (PARR) coupled with a magnetic stirrer. Typically, ortho-substituted aniline (1 mmol), CoNi@C (100 mg), and ethanol (5 mL) were loaded into the reactor. The autoclave was closed and then charged with CO_2 to 15 bar, further with H_2 up to a total pressure of 30 bar at room temperature. Subsequently, the reactor was heated at 115 °C with stirring. After 18-h the reactor was cooled down and the gas inside was carefully vented. The crude reaction mixture was centrifuged with ethyl acetate to separate the catalyst and then concentrated using a rotary evaporator and purified by column chromatography using ethyl acetate/dichloromethane to give the isolated compound that was characterized by ^{1}H NMR, and ^{13}C NMR.

3.4. Catalysis of CO_2 Methanation

The methanation of CO_2 was performed using a fixed bed reactor (PID Microactivity-Effi reactor) at 375 °C and 30 bar. An Inconel reactor tube with an internal diameter of 8 mm was used to host the reaction. The catalyst sample (200 mg) was pelletized in a pellet size of 100–300 microns and then loaded in between two layers of quartz wool inside the reactor tube. The sample was preheated at a ramping rate of 15 °C/min to 550 °C under a continuous flow of N_2 gas (20 mL/min) for 30 min. After that, the sample was reduced under H_2 (3 mL/min) and N_2 (20 mL/min) flow for another 30 min. After the reduction, the sample was cooled down to 70 °C, pressurized with the reactant feed to 30 bar, and then heated to reaction temperature (375 °C) to carry on the reaction. The reactant feed was a mixture of CO_2 and H_2 with an H_2 to CO_2 ratio of three, and the feed flow rate was kept at 15 mL/min with gas hourly space velocity (GHSV) of 4500 mL/(g·h^{-1}). The quantitative and qualitative analysis was performed using gas chromatography (Shimadzu, Kyoto, Japan, GC-2014) equipped with one thermal conductivity detector (TCD) and one flammable ionization detector (FID).

4. Conclusions

In conclusion, we have prepared a bimetallic nanoalloy CoNi@C derived from the CoNiBTC MOF that acts as a good catalyst for the synthesis of various substituted benzimidazoles from the corresponding *o*-phenylenediamine in a good yield (78–82%), in the presence of a mixture of CO_2 and H_2 at elevated temperature and pressure. The same catalyst was also utilized for the 99.7% selective methanation of CO_2. Thus, we have employed bimetallic BTC MOF as a precursor in the synthesis of functional nanomaterials with a controlled structure and customized compositions, encased in carbon shells with a high dispersion that boosted their catalytic activity.

Supplementary Materials: The following supporting information can be downloaded at https://www.mdpi.com/article/10.3390/catal13020357/s1, Section S1: Characterization of different ratios of CoNiBTC and CoNi@C; Section S2: ^{1}H and ^{13}C NMR of Benzimidazole products; Section S3: ^{1}H NMR spectra of Benzimidazole products; Section S4: Regeneration of Catalyst after Reaction; and Section S5: Methanation Reaction. References [37–49] are cited in the Supplementary Materials.

Author Contributions: Conceptualization, A.H., M.A.S., B.H. and M.H.Z.; methodology, A.H., M.A.S., B.H. and M.H.Z.; investigation, A.H.; resources, A.H., M.A.S., M.U. and M.H.Z.; writing—original draft preparation, A.H.; writing—review and editing, A.H., M.A.S., B.H., M.U. and M.H.Z.; supervision, A.H., M.A.S. and M.H.Z.; formal analysis, A.H., M.A.S., and B.H.; funding acquisition, A.H. All authors have read and agreed to the published version of the manuscript.

Funding: King Fahd University of Petroleum and Minerals: ORCP2390.

Data Availability Statement: Not Available.

Acknowledgments: We acknowledge the Interdisciplinary Research Center for Hydrogen and Energy Storage (IRC-HES) for their continued support. This research was supported by Saudi Aramco Chair Professor Project at KFUPM ORCP2390.

Conflicts of Interest: The authors declare that there are no conflict of interest.

References

1. Younas, M.; Loong, L.L.; Bashir, M.J.K.; Nadeem, H.; Shehzad, A.; Sethupathi, S. Recent Advancements, Fundamental Challenges, and Opportunities in Catalytic Methanation of CO_2. *Energy Fuels* **2016**, *30*, 8815–8831. [CrossRef]
2. Mardani, A.; Streimikiene, D.; Cavallaro, F.; Loganathan, N.; Khoshnoudi, M. Carbon dioxide (CO_2) emissions and economic growth: A systematic review of two decades of research from 1995 to 2017. *Sci. Total. Environ.* **2019**, *649*, 31–49. [CrossRef]
3. Gielen, D.; Boshell, F.; Saygin, D.; Bazilian, M.D.; Wagner, N.; Gorini, R. The role of renewable energy in the global energy transformation. *Energy Strategy Rev.* **2019**, *24*, 38–50. [CrossRef]
4. Younas, M.; Sohail, M.; Leong, L.K.; Bashir, M.J.K.; Sumathi, S. Feasibility of CO_2 adsorption by solid adsorbents: A review on low-temperature systems. *Int. J. Environ. Sci. Technol.* **2016**, *13*, 1839–1860. [CrossRef]
5. Lewis, N.S.; Nocera, D.G. Powering the planet: Chemical challenges in solar energy utilization. *Proc. Natl. Acad. Sci. USA* **2006**, *103*, 15729–15735. [CrossRef]
6. Wang, S.; Wang, X. Imidazolium Ionic Liquids, Imidazolylidene Heterocyclic Carbenes, and Zeolitic Imidazolate Frameworks for CO_2 Capture and Photochemical Reduction. *Angew. Chem. Int. Ed.* **2016**, *55*, 2308–2320. [CrossRef]
7. Listorti, A.; Durrant, J.; Barber, J. Solar to fuel. *Nat. Mater.* **2009**, *8*, 929–930. [CrossRef]
8. Wang, S.; Guan, B.Y.; Lou, X.W. Rationally designed hierarchical N-doped carbon@$NiCo_2O_4$ double-shelled nanoboxes for enhanced visible light CO_2 reduction. *Energy Environ. Sci.* **2018**, *11*, 306–310. [CrossRef]
9. Sakakura, T.; Choi, J.C.; Yasuda, H. Transformation of Carbon Dioxide. *Chem. Rev.* **2007**, *107*, 2365–2387. [CrossRef]
10. Mazari, S.A.; Hossain, N.; Basirun, W.J.; Mubarak, N.M.; Abro, R.; Sabzoi, N.; Shah, A. An overview of catalytic conversion of CO_2 into fuels and chemicals using metal organic frameworks. *Process Saf. Environ. Prot.* **2021**, *149*, 67–92. [CrossRef]
11. Wang, Q.; Hu, K.; Gao, R.; Zhang, L.; Wang, L.; Zhang, C. Research on the Growth Mechanism of $PM_{2.5}$ in Central and Eastern China during Autumn and Winter from 2013–2020. *Atmosphere* **2022**, *13*, 1–38.
12. Helal, A.; Alahmari, F.; Usman, M.; Yamani, Z.H. Chalcopyrite UiO-67 Metal-Organic Framework Composite for CO_2 Fixation as Cyclic Carbonates. *J. Environ. Chem. Eng.* **2022**, *10*, 108061–108068. [CrossRef]
13. Helal, A.; Shah, S.S.; Usman, M.; Khan, M.Y.; Aziz, M.A.; Rahman, M.M. Potential Applications of Nickel-Based Metal-Organic Frameworks and their Derivatives. *Chem. Rec.* **2022**, e202200055. [CrossRef]
14. Trickett, C.A.; Helal, A.; Al-Maythalony, B.A.; Yamani, Z.H.; Cordova, K.E.; Yaghi, O.M. The chemistry of metal-organic frameworks for CO_2 capture, regeneration and conversion. *Nat. Rev. Mater.* **2017**, *2*, 17045–17069. [CrossRef]
15. He, M.Y.; Sun, Y.H.; Han, B.X. Green Carbon Science: Scientific Basis for Integrating Carbon Resource Processing, Utilization, and Recycling. *Angew. Chem. Int. Ed.* **2013**, *52*, 9620–9633. [CrossRef]
16. Yang, Z.Z.; He, L.N.; Gao, J.; Liu, A.H.; Yu, B. Carbon dioxide utilization with C–N bond formation: Carbon dioxide capture and subsequent conversion. *Energy Environ. Sci.* **2012**, *5*, 6602–6639. [CrossRef]
17. Navarrete-Vazquez, G.; Cedillo, R.; Hernandez-Campos, A.; Yepez, L.; Hernandez-Luis, F.; Valdez, J.; Morales, R.; Cortes, R.; Hernandez, M.; Castillo, R. Synthesis and antiparasitic activity of 2-(trifluoromethyl) benzimidazole derivatives. *Biorg. Med. Chem. Lett.* **2001**, *11*, 187–190. [CrossRef]
18. Derayea, S.M.; Ali, H.R.H.; Hamad, A.A.; Ali, R.J. Application of silver nanoparticles for the spectrophotometric determination of three benzimidazole anthelmintic drugs in their pharmaceutical preparations. *Appl. Pharm. Sci.* **2017**, *7*, 76–82.
19. Khatun, R.; Biswas, S.; Biswas, I.H.; Riyajuddin, S.; Haque, N.; Ghosh, K.; Islam, S.M. Cu-NPs@COF: A potential heterogeneous catalyst for CO_2 fixation to produce 2-oxazolidinones as well as benzimidazoles under moderate reaction conditions. *J. CO2 Util.* **2020**, *40*, 101180–101191. [CrossRef]
20. Wang, F.; He, S.; Chen, H.; Wang, B.; Zheng, L.; Wei, M.; Evans, D.G.; Duan, X. Active Site Dependent Reaction Mechanism over Ru/CeO_2 Catalyst toward CO_2 Methanation. *J. Am. Chem. Soc.* **2016**, *138*, 6298–6305. [CrossRef]
21. Tsiotsias, A.I.; Charisiou, N.D.; Yentekakis, I.V.; Goula, M.A. Bimetallic Ni-Based Catalysts for CO_2 Methanation: A Review. *Nanomaterials* **2021**, *11*, 1–34. [CrossRef]
22. Guo, Y.; Mei, S.; Yuan, K.; Wang, D.-J.; Liu, H.-C.; Yan, C.-H.; Zhang, Y.-W. Low-Temperature CO2 Methanation over CeO2-Supported Ru. *ACS Catal.* **2018**, *8*, 6203–6215. [CrossRef]
23. Yu, B.; Zhang, H.Y.; Zhao, Y.F.; Chen, S.; Xu, J.L.; Huang, C.L.; Liu, Z.M. Cyclization of *o*-phenylenediamines by CO_2 in the presence of H_2 for the synthesis of benzimidazoles. *Green Chem.* **2013**, *15*, 95–99. [CrossRef]
24. Abdel-Mageed, A.M.; Widmann, D.; Olesen, S.E.; Chorkendorff, I.; Biskupek, J.; Behm, R.J. Selective CO Methanation on Ru/TiO_2 Catalysts. *ACS Catal.* **2015**, *5*, 6753–6763. [CrossRef]

25. Tsang, S.; Claridge, J.B.; Green, M. Recent advances in the conversion of methane to synthesis gas. *Catal. Today* **1995**, *23*, 3–15. [CrossRef]
26. Sankar, M.; Dimitratos, N.; Miedziak, P.J.; Wells, P.P.; Kiely, C.J.; Hutchings, G.J. Designing bimetallic catalysts for a green and sustainable future. *Chem. Soc. Rev.* **2012**, *41*, 8099–8139. [CrossRef]
27. Qin, N.; Pan, A.; Yuan, J.; Ke, F.; Wu, X.; Zhu, J.; Liu, J.; Zhu, J. One-Step Construction of a Hollow Au@Bimetal-Organic Framework Core-Shell Catalytic Nanoreactor for Selective Alcohol Oxidation Reaction. *ACS Appl. Mater. Interfaces* **2021**, *13*, 12463–12471. [CrossRef]
28. Chaikittisilp, W.; Ariga, K.; Yamauchi, Y.J. A new family of carbon materials: Synthesis of MOF-derived nanoporous carbons and their promising applications. *Mater. Chem. A* **2013**, *1*, 14–19. [CrossRef]
29. Lin, X.; Wang, S.; Tu, W.; Hu, Z.; Ding, Z.; Hou, Y.; Dai, W. MOF-derived hierarchical hollow spheres composed of carbon-confined Ni nanoparticles for efficient CO_2 methanation. *Catal. Sci. Technol.* **2019**, *9*, 731–738. [CrossRef]
30. He, J.; Zhang, Y.; Pan, Q.; Yu, J.; Xu, R. Three metal-organic frameworks prepared from mixed solvents of DMF and HAc. *Microporous Mesoporous Mater.* **2006**, *90*, 145–152. [CrossRef]
31. Bavykina, A.; Kolobov, N.; Khan, I.S.; Bau, J.A.; Ramirez, A.; Gascon, G. Metal–Organic Frameworks in Heterogeneous Catalysis: Recent Progress, New Trends, and Future Perspectives. *Chem. Rev.* **2020**, *120*, 8468–8535. [CrossRef]
32. Qin, L.; Li, Y.; Liang, F.; Li, L.; Lan, Y.; Li, Z.; Lu, X.; Yang, M.; Ma, D. A microporous 2D cobalt-based MOF with pyridyl sites and open metal sites for selective adsorption of CO_2. *Microporous Mesoporous Mater.* **2022**, *341*, 112098. [CrossRef]
33. Hamza Fakeeha, A.; Arafat, Y.; Aidid Ibrahim, A.; Shaikh, H.; Atia, H.; Elhag Abasaeed, A.; Armbruster, U.; Sadeq Al-Fatesh, A. Highly Selective Syngas/H_2 Production via Partial Oxidation of CH_4 Using (Ni, Co and Ni–Co)/ZrO_2–Al_2O_3 Catalysts: Influence of Calcination Temperature. *Processes* **2019**, *7*, 141. [CrossRef]
34. Long, J.; Shen, K.; Chen, L.; Li, Y.J. Multimetal-MOF-derived transition metal alloy NPs embedded in an N-doped carbon matrix: Highly active catalysts for hydrogenation reactions. *Mater. Chem. A* **2016**, *4*, 10254–10262. [CrossRef]
35. Li, Y.; Wang, H.; Jiang, X.; Zhu, J.; Liu, Z.; Guo, X.; Song, C. A short review of recent advances in CO_2 hydrogenation to hydrocarbons over heterogeneous catalysts. *RSC Adv.* **2018**, *8*, 7651–7669. [CrossRef] [PubMed]
36. Yaghi, O.M.; Li, H.; Groy, T.L. Construction of Porous Solids from Hydrogen-Bonded Metal Complexes of 1,3,5-Benzenetricarboxylic acid. *J. Am. Chem. Soc.* **1996**, *118*, 9096–9101. [CrossRef]
37. Zhao, W.; Li, H.; Li, Y.; Long, J.; Xu, Y.; Yang, S. Low-cost acetate-catalyzed efficient synthesis of benzimidazoles using ambient CO_2 as a carbon source under mild conditions. *Sustain. Chem. Pharm.* **2020**, *17*, 100276. [CrossRef]
38. Hao, L.; Zhao, Y.; Yu, B.; Zhang, H.; Xu, H.; Liu, Z. Au catalyzed synthesis of benzimidazoles from 2-nitroanilines and CO_2/H_2. *Green Chem.* **2014**, *16*, 3039. [CrossRef]
39. Biswas, I.H.; Biswas, S.; Islam, M.S.; Riyajuddin, S.; Sarkar, P.; Ghosh, K.; Islam, S.M. Catalytic synthesis of benzimidazoles and organic carbamates using a polymer supported zinc catalyst through CO_2 fixation. *New J. Chem.* **2019**, *43*, 14643. [CrossRef]
40. Ke, Z.; Yu, Z.; Wang, H.; Xiang, J.; Han, J.; Wu, Y.; Liu, Z.; Yang, P.; Liu, Z. Cobalt-catalyzed synthesis of N-containing heterocycles via cyclization of ortho-substituted anilines with CO_2/H_2. *Green Chem.* **2019**, *21*, 1695. [CrossRef]
41. Phatake, V.V.; Bhanage, B.M. Cu@UgC_3N_4 Catalyzed Cyclization of *o*-Phenylenediamines for the Synthesis of Benzimidazoles by Using CO_2 and Dimethylamine Borane as a Hydrogen. *Catal. Lett.* **2019**, *149*, 347. [CrossRef]
42. Rasal, K.B.; Yadav, G.D. One-pot synthesis of benzimidazole using DMF as a multitasking reagent in presence $CuFe_2O_4$ as catalyst. *Catal. Today* **2018**, *309*, 51. [CrossRef]
43. Mihet, M.; Dan, M.; Barbu-Tudoran, L.; Lazar, M.D. CO_2 Methanation Using Multimodal Ni/SiO_2 Catalysts: Effect of Support Modification by MgO, CeO_2, and La_2O_3. *Catalysts* **2021**, *11*, 443. [CrossRef]
44. Zhou, G.; Liu, H.; Xing, Y.; Xu, S.; Xie, H.; Xiong, K. CO2 hydrogenation to methane over mesoporous Co/SiO_2 catalysts: Effect of structure. *J. CO2 Util.* **2018**, *26*, 221. [CrossRef]
45. Liu, H.; Xu, S.; Zhou, G.; Xiong, K.; Jiao, Z.; Wang, S. CO2 hydrogenation to methane over Co/KIT-6 catalysts: Effect of Co content. *Fuel* **2018**, *217*, 570–576. [CrossRef]
46. Pieta, I.S.; Lewalska-Graczyk, A.; Kowalik, P.; Antoniak-Jurak, K. CO_2 Hydrogenation to Methane over Ni-Catalysts: The Effect of Support and Vanadia Promoting. *Catalysts.* **2021**, *11*, 433. [CrossRef]
47. Varvoutis, G.; Lykaki, M.; Stefa, S.; Papista, E.; Carabineiro, S.A.; Marnellos, G.E.; Konsolakis, M. Remarkable efficiency of Ni supported on hydrothermally synthesized CeO_2 nanorods for low-temperature CO2 hydrogenation to methane. *Catal. Commun.* **2020**, *142*, 106036. [CrossRef]
48. Franken, T.; Terreni, J.; Borgschulte, A.; Heel, A. Solid solutions in reductive environment–A case study on improved CO_2 hydrogenation to methane on cobalt based catalysts derived from ternary mixed metal oxides. *J. Catal.* **2020**, *382*, 385. [CrossRef]
49. Dong, T.; Liu, X.; Tang, Z.; Yuan, H.; Jiang, D.; Wang, Y.; Liu, Z.; Zhang, X.; Huang, S.; Liu, H.; et al. Ru Decorated TiO_x Nanoparticles via Laser Bombardment for Photothermal Co-catalytic CO_2 Hydrogenation to Methane with High Selectivity. *Appl. Catal B Environ.* **2022**, *326*, 122176. [CrossRef]

Disclaimer/Publisher's Note: The statements, opinions and data contained in all publications are solely those of the individual author(s) and contributor(s) and not of MDPI and/or the editor(s). MDPI and/or the editor(s) disclaim responsibility for any injury to people or property resulting from any ideas, methods, instructions or products referred to in the content.